厚生労働科学研究費補助金（第３次対がん総合戦略研究事業）

分担研究報告書

分担研究者：　柳澤　聖（名古屋大学大学院医学系研究科分子腫瘍学分野・講師）

分担研究項目：　CIMに関する研究開発及び新規標的分子の探索・同定

研究要旨

本年度は、我々が同定した肺がん浸潤・転移に重要な働きを有するCIMの細胞運動性に関連する機能を明らかとする目的で、プロテオミクス技術を応用して、網羅的に結合蛋白の探索を進めた。本年度は、CIMの持つ細胞運動能の制御機能の詳細を明らかとすることによって、転移抑制を目指した創薬研究開発への基盤を構築すべく検討を進めた。CIMアフィニティーカラムを用いて、LNM35細胞中に存在するCIM結合分子の精製を行い、さらに質量分析装置を応用した精密定量法であるMRM解析系を用いた検証を進めることにより、11種類の分子とCIMとの結合を確認することに成功した。これら分子の多くは、アクチン重合や細胞骨格構成について重要な働きを果たすものであり、CIMが細胞運動能・浸潤能の制御に深く関与する事を示唆するものと考えた。

さらに、我々が樹立したヒト肺がんの転移研究モデルLNM35株と、最新のプロテオミクス解析技術を駆使する事により、分子標的薬の創薬開発に有利なリン酸化蛋白プロファイル解析を遂行し、これまでに30,000以上のペプチドのリン酸化に関する発現情報の取得を完了し、リン酸化レベルに有意な差異のある数百か所のリン酸化サイトを同定することに成功しており、今後、転移能の獲得に関わるキナーゼ及びフォスファターゼの同定へ繋がるものと期待される。

A. 研究目的

先進諸国におけるがん死亡原因の第一位を占める代表的な難治癌である肺がんの病態の本態は浸潤・転移である。すなわち、その分子機構を詳細に解明し、取得された知見に基づいた診断・治療法の開発を進める事により、飛躍的な治癒率の向上につながる事が期待される。

これまでに、我々が優位性を有するプロテオミクスとバイオインフォマティクス技術を、我々が確立した極めて高い血行性及びリンパ行性転移を再現可能なヒト肺がん転移研究モデル（NCI-H460-LNM35株。以下LNM35株）(Kozaki K, et al. Cancer Res 2000; Kozaki K, et al. Oncogene 2001; Tomida S, et al. Oncogene 2007) とともに活用する事により、新規肺がん転移関連遺伝子CIM（cancer invasion and metastasis）の単離・同定に成功すると共に、CIMが、低酸素ストレス応答並びに小胞体ストレス応答シグナル伝達（UPR, unfolded protein response）を制御する事により、不良な微小環境における遠隔転移腫瘍細胞

の生存に深く寄与する事を明らかとしてきた。

本研究では、CIMの担う、さらなる肺がん細胞の運動能・浸潤能獲得の過程における重要な機能を明らかとすることで、それらの知見を新規のがん診断治療法へ応用することをめざしている。また、さらなる分子標的の探索・同定を、分子標的薬の創薬開発に有利なキナーゼに焦点を絞ったプロテオミクス解析により探索・同定し、LNM35株を用いた生化学的・細胞生物学的な機能の検証、肺癌臨床検体の網羅的発現情報データとの統合的バイオインフォマティクス解析を進めることにより、新たな分子標的薬開発の基盤構築を目指している。

B. 方法

CIM結合蛋白候補の網羅的探索

GST蛋白融合CIM発現バキュロウィルスベクターを作成し、Sf9細胞を用いたCIM遺伝子産物の大量精製系を確立した。精製されたCIM遺伝子産物をグルタチオンビーズと結合させる事によりCIMアフィニティーカラムを作成した。高転移性LNM35細胞より抽出した蛋白試料からCIMアフィニティーカラムを用いて、CIM結合分子群の精製を行った。精製されたCIM結合蛋白を対照試料(グルタチオンビーズにLNM35細胞抽出液を添加した後に、同手順に従い精製)とともに、還元・アルキル化処理の後に、トリプシンを用いた蛋白消化を行って、それぞれの蛋白試料からペプチド試料を得た。非放射性安定同位体ペプチド標識試薬であるiTRAQを用いて取得されたペプチド試料の標識化を行い、ナノフロー液体クロマトグラフィーと質量分析装置を応用することにより、両試料における網羅的発現プロファイルの比較定量解析を行った。

MRM技術を用いたin vitro結合の検証

同定されたCIM結合候補分子群を対象として、質量分析装置を応用した精密定量法であるMRM解析系を用いた、CIMアフィニティーカラムにより LNM35株から精製した試料に対する検証を進めた。

LNM35細胞内におけるCIMとの結合の検証

LNM35細胞を用いて、myc標識CIMを外来性に発現させ、ピューロマイシンを用いて外来性CIM発現細胞をセレクションの後、蛋白を抽出し、抗 myc 抗体を用いた pull down を行った。CIM 共沈分子に対して MRM 解析系を用いた精密定量解析を行い、CIM結合候補蛋白の存在に関する検討を行った。

LNM35-N15細胞間で発現変動を認めるリン酸化蛋白の網羅的探索

LNM35並びにN15株より蛋白を抽出し、還元・アルキル化処理の後に、トリプシンを用いた蛋白消化を行って、それぞれのペプチド試料を得た。独自に調整した鉄結合ビーズを用いてiMAC(immobility metal affinity column)を作成し、それぞれのペプチド試料より、リン酸化ペプチドの大量精製・濃縮を行った。精製・濃縮リン酸化ペプチド試料は、さらに、iTRAQ試薬を用いて標識化を行い、ナノフロー液体クロマトグラフィーと質量分析装置を駆使した解析を行うことにより、網羅的比較定量発現プロファイルの取得を進めた。

C. 結果

I. CIM及びそのシグナリング分子を標的とした検討:

CIMを標的とするshort-hairpin RNA発現ベクターを用いて、高転移性LNM35細胞において、恒常的にCIMの発現を抑制する事により、顕著な細胞運動能・浸潤能の抑制が引き起こされる(図1)。これは、我々が明らかとした、CIMの持つ、ERに局在しがん細胞が周囲の微小環境から絶えず受け続ける低酸素、

【図1】CIMのLNM35細胞の運動能維持への寄与

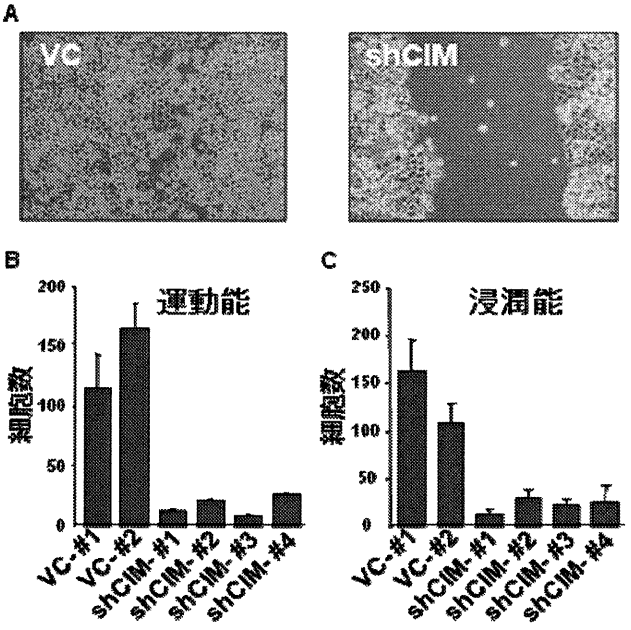

A. CIM発現抑制LNM35細胞における細胞運動能の低下（スクラッチアッセイ）B. CIM発現抑制LNM35細胞における細胞運動能の低下C. CIM発現抑制LNM35細胞における細胞浸潤能の低下

或いは低栄養などのストレスに対する耐性を付与する機能では説明がつかず、未知の機能の存在が示唆される。

そこで、CIMの持つ細胞運動・浸潤能の制御機能の詳細を明らかとすることによって、転移抑制を目指した創薬研究開発への基盤を構築すべく検討を進めた。まず、バキュロウィルス・Sf9細胞を用いて、CIM遺伝子産物の大量精製系を確立し、CIM遺伝子産物カラムの作成を行った（図2）。LNM35細胞より抽出した蛋白試料中に存在するCIM結合分子の精製を行った。さらに、酵素消化後にタンデムナノ液体クロマトグラフィーとタンデム質量分析器を用いた網羅的な蛋白発現解析を行った結果、45種類のCIM結合候補分子を同定した。引き続いてこれらの分子群を対象として、質量分析装置を応用した精密定量法であるMRM解析系の構築を行い、上記と同様のバキュロウィルス・Sf9細胞を用いて作成したCIMアフィニティーカラムにより、LNM35株から精

【図2】CIM結合タンパク質の網羅的探索

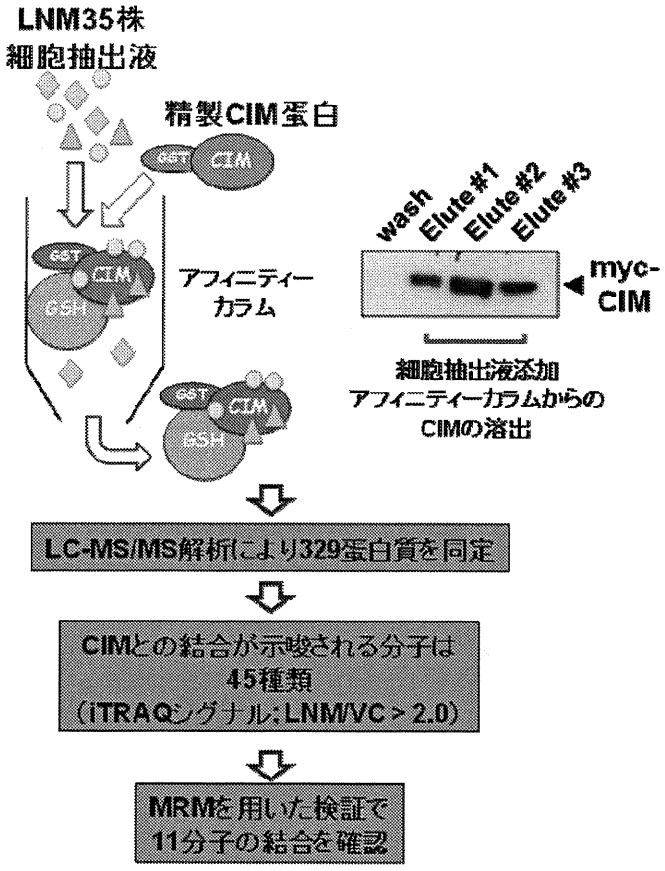

ペプチド標識試薬iTRAQと質量分析装置を応用したCIM結合タンパク質の網羅的比較定量解析法の概略

製した試料に対する検証を進め、11種類の分子とCIMとの結合を確認することに成功した。これら分子群が共通して有する機能を推定する目的で、GO解析を進めた結果、細胞骨格制御、或いは細胞運動能の制御機構との関連性が示唆され、CIMがこれらの分子群と共作用して、浸潤・転移の制御に寄与する事が示唆された（表1）。

【表1】GO解析が示唆するCIM結合分子の機能

Molecular function	P value
cytoskeleton organization	0.0036
cell adhesion molecule binding	0.0206
actin filament regulation	0.0222
SH3 domain binding	0.0646

さらなる検証として、myc標識CIMを外来性にLNM35株で発現させ、抗myc抗体を用いたpull downを行い、共沈分子に対してMRM解析を加えたところ、細胞内おけるCIMと候補分子群の結合が示唆される結果を得た(図3)。

【図3】CIM結合候補分子のMRMによる検証

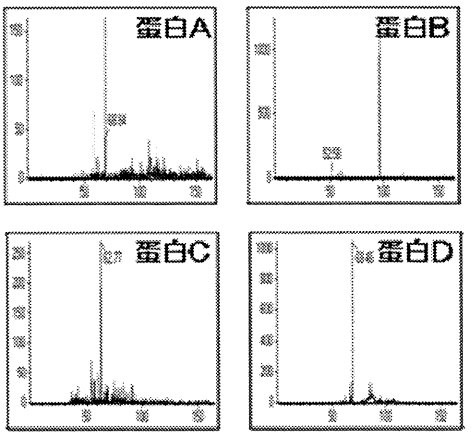

myc-CIMを外来性に導入したLNM35細胞を用いて、CIM共沈蛋白を精製し、候補分子を標的としたMRM解析系を用いてその存在を確認

現在、これらの分子の発現変化による肺がん細胞の運動・浸潤能への影響について検討を進めると共に、肺がん臨床検体におけるこれら分子群の発現と臨床情報との関連について検討を進めつつある。また、機能阻害の標的となり得るドメインを同定すべく、CIM部分欠失変異体を用いた分子間結合に関する検討を進めつつある。

II. LNM35株のプロテオミクス解析による新規分子標的の探索・同定と応用:

LNM35 株という極めて有用なヒト肺がんの転移研究モデル系と、最新のプロテオミクス解析技術の両者を併せ持つ本研究グループの優位性を生かし、さらなる分子標的の探索・同定も進めた。本年度は、分子標的薬の創薬開発に有利なキナーゼを念頭に、高転移性亜株LNM35 株と低転移性親株 N15 株を用いてリン酸化蛋白の網羅的発現プロファイル比較を進めた。これまでに 30,000 以上のペプチドのリン酸化に関する発現情報の取得を完了し、リン酸化レベルに有意な差異のある数百か所のリン酸化サイトを同定することに成功している。今後、基質のモチーフ解析などを進める事により、転移能の獲得に関わるキナーゼ及びフォスファターゼの同定へと結び付け、新たな肺癌治療開発へと発展させることを目指す。

D. 健康危険情報

特記すべき事項無し

E. 研究発表

1. Hosono Y, Yamaguchi T, Mizutani E, Yanagisawa K, Arima C, Tomida S, Shimada Y, Hiraoka M, Kato S, Yokoi K, Suzuki M, Takahashi T. MYBPH, a transcriptional target of TTF-1, inhibits ROCK1, and reduces cell motility and metastasis. ***EMBO J***, 31:481-93, 2012.
2. Yamaguchi T, Yanagisawa K, Sugiyama R, Hosono Y, ShimadaY, Arima C, Kato S, Tomida S, Suzuki M, Osada H, Takahashi T: NKX2-1/TITF1/TTF-1-induced ROR1 is required to sustain EGFR survival signaling in lung adenocarcinoma. ***Cancer Cell*** (in press).
3. Nishikawa E, Osada H, Okazaki Y, Arima C, Tomida S, Tatematsu Y, Taguchi A, Shimada Y, Yanagisawa K, Yatabe Y, Toyokuni S, Sekido Y, Takahashi T. miR-375 is activated by ASH1 and inhibits YAP1 in a lineage-dependent manner in lung cancer. ***Cancer Res,*** 71:6165-73, 2011.

F. 学会発表

1. Yanagisawa K, Kato S, Hotta N, Nakamura S, Takahashi T: CKAP4, novel malignant pulmonary mesothelioma-related gene, regulates eIF2α and cellular stress-response. 70th Annual Meeting of the Japanese Cancer Association (English oral session), Nagoya, October 3-5, 2011.

G. 知的財産権の出願・登録状況

a. 特許出願
b. 実用新案登録
c. その他

いずれも、特記すべき事項無し

IV. 研究成果の刊行に関する一覧表

研究成果の刊行に関する一覧

発表者氏名	論文タイトル名	発表誌名	巻号	ページ	出版年
Hosono Y, Yamaguchi T, Mizutani E, Yanagisawa K, Arima C, Tomida S, Shimada Y, Hiraoka M, Kato S, Yokoi K, Suzuki M, Takahashi T	MYBPH, a transcriptional target of TTF-1, inhibits ROCK1, and reduces cell motility and metastasis.	EMBO J.	31	481-493	2012
Yamaguchi T, Yanagisawa K, Sugiyama R, Hosono Y, ShimadaY, Arima C, Kato S, Tomida S, Suzuki M, Osada H, Takahashi T	NKX2-1/TITF1/TTF-1-induced ROR1 is required to sustain EGFR survival signaling in lung adenocarcinoma.	Cancer Cell		in press	
Fujii M, Toyoda T, Nakanishi H, Yatabe Y, Sato A, Matsudaira Y, Ito H, Murakami H, Kondo Y, Kondo E, Hida T, Tsujimura T, Osada H, Sekido Y	TGF-β synergizes with defects in the Hippo pathway to stimulate human malignant mesothelioma growth.	J. Exp. Med.		in press	
Mizuno T, Murakami H, Fujii M, Ishiguro F, Tanaka I, Kondo Y, Akatsuka S, Toyokuni S, Yokoi K, Osada H, Sekido Y	YAP induces malignant mesothelioma cell proliferation by upregulating transcription of cell cycle promoting genes.	Oncogene		in press	
Endo M, Nakano M, Kadomatsu T, Fukuhara S, Kuroda H, Mikami S, Hato T, Aoi J, Horiguchi H, Miyata K, Odagiri H, Masuda T, Harada M, Horio H, Hishima T, Nomori H, Ito T Yamamoto Y, Minami T, Okada S, Takahashi T, Mochizuki N, Iwase H, Oike Y.	A critical role for tumor cell-derived angiopoientin-like protein 2 in metastasis.	Cancer Res.		in press	
Ishiguro F, Murakami H, Mizuno T, Fujii M, Kondo Y, Usami N, Yokoi K, Osada H, Sekido Y	Activated leukocyte cell adhesion molecule (ALCAM) promotes malignant phenotypes of malignant mesothelioma.	J. Thorac. Oncol.		in press	

Suda K, Tomizawa K, Osada H, Maehara Y, Yatabe Y, Sekido Y, Mitsudomi T	Conversion from the "oncogene addiction" to "drug addiction" by intensive inhibition of the EGFR and MET in lung cancer with activating EGFR mutation.	Lung Cancer		in press	
Nishikawa E*, Osada H*, Okazaki Y, Arima C, Tomida S, Tatematsu Y, Taguchi A, Shimada Y, Yanagisawa K, Yatabe Y, Toyokuni S, Sekido Y, Takahashi T (*equal contributors)	miR-375 is activated by ASH1 and inhibits YAP1 in a lineage-dependent manner in lung cancer.	Cancer Res.	71	6165-6173	2011
Matsuyama Y, Suzuki M, Arima C, Huang QM, Tomida S, Takeuchi T, Sugiyama R, Itoh Y, Yatabe Y, Goto H, and Takahashi T	Proteasomal non-catalytic subunit PSMD2 as a potential therapeutic target in association with various clinicopathologic features in lung adenocarcinomas.	Mol. Carcinog.	50	301-309	2011
Shimamura T, Imoto S, Shimada Y, Hosono, Y., Niida, A., Nagasaki, M., Yamaguchi, R., Takahashi, T., Miyano, S	A novel network profiling analysis reveals system changes in epithelial-mesenchymal transition.	PLoS ONE	6	e20804. doi:10.1371 /journal.pon e.0020804	2011
Osada H, Takahashi T	let-7 and miR-17-92: small-sized major players in lung cancer development.	Cancer Sci.	102	9-17	2011
Murakami H, Mizuno T, Taniguchi T, Fujii M, Ishiguro F, Fukui T, Akatsuka S, Horio Y, Hida T, Kondo Y, Toyokuni S, Osada H, Sekido Y	LATS2 is a tumor suppressor gene of malignant mesothelioma.	Cancer Res.	71	873-883	2011
Sides M, Klingsberg RC, Shan B, Gordon KA, Nguyen HT, Lin Z, Takahashi T; Flemington, E.K., and Lasky, J.A.	The Epstein-Barr virus LMP 1 and TGF-β1 synergistically induce EMT in lung epithelial cells.	Am J. Resp. Cell Mol. Biol.	44	852-862	2011

Ju HX, An B, Okamoto Y, Shinjo K, Kanemitsu Y, Komori K, Hirai T, Shimizu Y, Sano T, Sawaki A, Tajika M, Yamao K, Fujii M, Murakami H, Osada H, Ito H, Takeuchi I, Sekido Y, Kondo Y:	Distinct profiles of epigenetic evolution between colorectal cancers with and without metastasis.	Am. J. Pathol.	178	1835-1846	2011
Attoub S, Hassan AH, Vanhoecke B, Iratni R, Takahashi T, Gaben AM, Bracke M, Awad S, Kamalboor JA, Al Sultan MAH, Arafat K, Gespach C, Petroianu G	Inhibition of cell survival, invasion, tumor growth and histone deacetylase activity by the dietary flavonoid luteolin in human epithelioid cancer cells.	Eur. J. Pharmacol.	651	18-25	2011
Mulder JE, Brien JF, Racz WJ, Takahashi T, Massey T	Mechanisms of amiodarone and desethylamiodarone cytotoxicity in non-transformed human peripheral lung epithelial cells.	J. Pharmacol. Exp. Ther.	336	551-559	2011
Travis WD, Brambilla E, Noguchi M, Nicholson AG, Geisinger KR, Yatabe Y, Beer DG, Powell CA, Eiely GJ, Van Schil PE, Garg, K, Austin JHM, Asamura H, Rusch, VW, Hirsch FR, Scagliotti G, MisudomiT, Huber RM, Ishikawa Y, Jett, J, Sanchez-Cespedes, M, Sculier, JP, Takahashi T, Tsuboi, M, Vansteenkiste J, Wistuba I, Yang, P-C, Aberle D, Brambilla C, Flieder D, Franklin W, Johnson B, Johnson D, Kerr K, Kuriyama K, Lee JS, Miller VA, pertersen I, Roggli V, Rosell R, Saijo N, Thunnissen E, Tsao M, Yankelewitz D	International Association for the Study of Lung Cancer/Amerian Thoracic Society/European Respiratory Society International Multidisciplinary Classification of lung adenocarcinoma.	J. Thorac. Oncol.	6	244-285	2011
Suda K, Tomizawa K, Fujii M, Murakami H, Osada H, Maehara Y, Yatabe Y, Sekido Y, Mitsudomi T	Epithelial to mesenchymal transition in an EGFR-mutant lung cancer cell line with acquired resistance to erlotinib.	J. Thorac. Oncol.	6	1152-1161	2011

Okamoto Y, Sawaki A, Ito S, Nishida T, Takahashi T, Toyota M, Suzuki H, Shinomura Y, Takeuchi I, Shinjo K, An B, Ito H, Yamao K, Fujii M, Murakami H, Osada H, Kataoka H, Joh T, Sekido Y, Kondo Y	Aberrant DNA methylation associated with aggressiveness of gastrointestinal stromal tumour.	GUT	61	392-401	2012

V. 研究成果の刊行物・別刷

The EMBO Journal (2012) 31, 481–493 | © 2012 European Molecular Biology Organization | All Rights Reserved 0261-4189/12
www.embojournal.org

THE EMBO JOURNAL

MYBPH, a transcriptional target of TTF-1, inhibits ROCK1, and reduces cell motility and metastasis

Yasuyuki Hosono[1,2], Tomoya Yamaguchi[1], Eri Mizutani[1], Kiyoshi Yanagisawa[1,3], Chinatsu Arima[1], Shuta Tomida[1], Yukako Shimada[1], Michiyo Hiraoka[1], Seiichi Kato[1], Kohei Yokoi[2], Motoshi Suzuki[1] and Takashi Takahashi[1,*]

[1]Division of Molecular Carcinogenesis, Center for Neurological Diseases and Cancer, Nagoya University Graduate School of Medicine, Nagoya, Japan, [2]Department of Thoracic Surgery, Nagoya University Graduate School of Medicine, Nagoya, Japan and [3]Institute for Advanced Research, Nagoya University, Nagoya, Japan

Cell migration driven by actomyosin filament assembly is a critical step in tumour invasion and metastasis. Herein, we report identification of *myosin binding protein H* (*MYBPH*) as a transcriptional target of *TTF-1* (also known as *NKX2-1 and TITF1*), a master regulator of lung development that also plays a role as a lineage-survival oncogene in lung adenocarcinoma development. MYBPH inhibited assembly competence-conferring phosphorylation of the myosin regulatory light chain (RLC) as well as activating phosphorylation of LIM domain kinase (LIMK), unexpectedly through its direct physical interaction with Rho kinase 1 (ROCK1) rather than with RLC. Consequently, MYBPH inhibited ROCK1 and negatively regulated actomyosin organization, which in turn reduced single cell motility and increased collective cell migration, resulting in decreased cancer invasion and metastasis. Finally, we also show that *MYBPH* is epigenetically inactivated by promoter DNA methylation in a fraction of *TTF-1*-positive lung adenocarcinomas, which appears to be in accordance with its deleterious functions in lung adenocarcinoma invasion and metastasis, as well as with the paradoxical association of *TTF-1* expression with favourable prognosis in lung adenocarcinoma patients.

The EMBO Journal (2012) **31**, 481–493. doi:10.1038/emboj.2011.416; Published online 15 November 2011
Subject Categories: cell & tissue architecture
Keywords: actomyosin; cytoskeleton; lung cancer; ROCK1

Introduction

Metastasis is thought to be initiated by disruption of cell–cell contact, followed by single cell migration. It is widely accepted that contractile motion of cancer cells is generated by assembly and consecutive contraction of actomyosin bundles (Lauffenburger and Horwitz, 1996; Friedl and Wolf, 2003; Hall, 2009). Collective cell migration has been shown to result from decreasing actomyosin contractility at the sites of cell–cell contact and plays a role in a range of developmental processes as well as cancer invasion (Christiansen and Rajasekaran, 2006; Hidalgo-Carcedo *et al*, 2011).

Non-muscle myosin II (NM II), a major component of the actomyosin cytoskeleton, comprising two non-muscle myosin heavy chains (NMHCs) and two essential myosin light chains (ELCs), as well as two regulatory light chains (RLCs) (Conti and Adelstein, 2008; Vicente-Manzanares *et al*, 2009). Emerging evidence indicates that NM II members, especially NM IIA, are crucially involved in cancer cell migration, invasion, and metastasis via bivalent binding to actin filaments (Betapudi *et al*, 2006; Huang *et al*, 2009; Medjkane *et al*, 2009). Rho kinase 1 (ROCK1), a downstream effecter of RhoA, is a major positive regulator of that process, which is thought to be executed through phosphorylation of RLC and subsequent unfolding of NM IIA into an assembly competent form capable of NM IIA dimer formation. In addition, ROCK1 phosphorylates LIM domain kinase (LIMK) and stabilizes actin filaments through inactivation of the actin-depolymerizing factor cofilin. Another member of the ROCK family, ROCK2, is abundantly and preferentially expressed in non-epithelial tissues such as the brain and muscles, and plays roles in phagocytosis and cell contraction (Etienne-Manneville and Hall, 2002; Riento and Ridley, 2003; Amano *et al*, 2010). However, how actomyosin organization in non-muscle cells is negatively regulated to counterbalance the positive regulatory function of ROCK1 largely remains to be elucidated.

TTF-1 is a lineage-specific transcription factor required for branching morphogenesis and physiological lung functions (Kimura *et al*, 1996). TTF-1 is also involved in pathological conditions of the lung. For example, TTF-1 expression is prominent in lung epithelial cells undergoing regeneration (White *et al*, 2001; Pogach *et al*, 2007). A major fraction of lung adenocarcinomas are also TTF-1 positive, which is suggested to reflect their derivation from the terminal respiratory unit (Yatabe *et al*, 2002; Takeuchi *et al*, 2006). We and others recently identified TTF-1 as a lineage-survival oncogene with focal amplification in lung adenocarcinomas (Kendall *et al*, 2007; Tanaka *et al*, 2007; Weir *et al*, 2007; Kwei *et al*, 2008). However, it is of note that *TTF-1* expression is associated with favourable prognosis in lung adenocarcinoma cases (Anagnostou *et al*, 2009). In the present study, we identified MYBPH as a transcriptional target of TTF-1, which provides a clue for elucidating the molecular mechanism related to how TTF-1 paradoxically inhibits cancer invasion and metastasis.

Results

MYBPH is directly transactivated by TTF-1

As an initial step towards a better understanding of transcriptomes regulated by *TTF-1*, microarray analysis was

*Corresponding author. Division of Molecular Carcinogenesis, Center for Neurological Diseases and Cancer, Nagoya University Graduate School of Medicine, 65 Tsurumai, Showa-ku, Nagoya 466-8550, Japan. Tel.: +81 52 744 2454; Fax: +81 52 744 2457;
E-mail: tak@med.nagoya-u.ac.jp

Received: 28 May 2011; accepted: 18 October 2011; published online: 15 November 2011

©2012 European Molecular Biology Organization

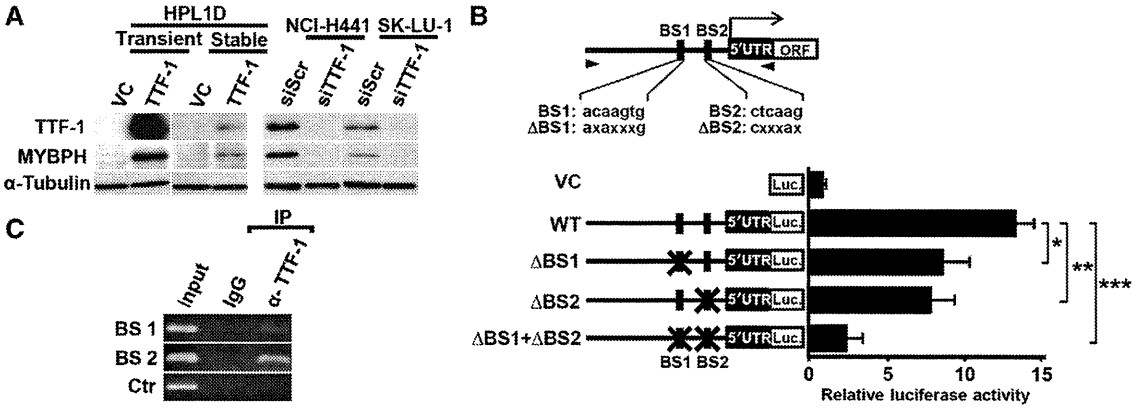

Figure 1 *MYBPH* is directly transactivated by TTF-1. (**A**) Western blot analysis showing induction of MYBPH in HPL1D cells transiently or stably transfected with TTF-1, as well as reduction by TTF-1 knockdown in NCI-H441 and SK-LU-1 cells. siScr, negative control siRNA; siTTF-1, siRNA against TTF-1. (**B**) Top panel: schematic diagram of *MYBPH* promoter region, BS1 and BS2, putative NKX2-5 and TTF-1 binding sites, respectively. Arrowheads, locations of primers used to amplify *MYBPH* promoter. Bottom panel: luciferase reporter analysis using HPL1D cells with transient TTF-1-expression. Three independent experiments were performed in triplicate. Bars, mean ± s.d.; $*P<0.05$; $**P<0.01$; $***P<0.005$. (**C**) Chromatin immunoprecipitation assay of NCI-H441 cells showing that TTF-1 protein binds to both BS1 and BS2. Figure source data can be found with the Supplementary data.

performed using an immortalized peripheral lung epithelial cell line, HPL1D (Masuda *et al*, 1997), which was transiently transfected with *TTF-1*. We consequently identified *MYBPH* as the most highly upregulated gene (Supplementary Figure S1) and confirmed its upregulation at the protein level by western blot analysis (Figure 1A). A dual-luciferase assay also revealed *TTF-1*-mediated transcriptional activation of *MYBPH* (Figure 1B; Supplementary Figure S2A), while a chromatin immunoprecipitation (ChIP) assay of NCI-H441 cells clearly demonstrated specific binding of TTF-1 with both potential TTF-1 binding sites in the *MYBPH* promoter (Figure 1C).

MYBPH expression is inactivated by the promoter CpG methylation

TTF-1 was invariably present in lung adenocarcinoma cell lines expressing MYBPH at readily detectable levels (Figure 2A), while a significant correlation between TTF-1 and MYBPH expression was also observed in the analysis of our previous microarray data set of 90 lung adenocarcinoma cases ($P=0.0051$; Figure 2B; Takeuchi *et al*, 2006). Interestingly, however, we noted that a considerable fraction of lung adenocarcinomas both *in vitro* and *in vivo* expressed low levels of *MYBPH* despite high *TTF-1* expression. Therefore, we evaluated whether aberrant DNA methylation of the *MYBPH* promoter was involved in silencing of *MYBPH*. Treatment with a DNA demethylating agent, 5-Aza-dC, significantly induced *MYBPH* in NCI-H358 and A427 cells (Figure 2C), while bisulphite sequencing analysis revealed clear distinctions in terms of dense DNA methylation surrounding the genuine TTF-1 binding site (BS2; Li *et al*, 1998), but not that for the TTF-1 homologue, NKX2-5 (BS1; Chen and Schwartz, 1995), in NCI-H358 and A427 cells (Figure 2D; Supplementary Figure S2B). Methylation-specific PCR (MSP) analysis using DNA from laser microdissected specimens further confirmed the presence of aberrant DNA methylation specifically in *MYBPH*$^-$/*TTF-1*$^+$ lung adenocarcinoma tissues *in vivo* (Figure 2E). The present findings thus indicate that *MYBPH* is a direct transcriptional target of *TTF-1*, which is inactivated by promoter DNA methylation in a considerable fraction of lung adenocarcinomas.

MYBPH reduces cell motility, invasion, and metastasis

NM II is a major component of the actomyosin cytoskeleton in non-muscle cells and crucially involved in cell migration (Betapudi *et al*, 2006; Conti and Adelstein, 2008; Huang *et al*, 2009; Medjkane *et al*, 2009; Vicente-Manzanares *et al*, 2009). The presence of inactivating promoter DNA methylation led us to speculate that *TTF-1*-induced *MYBPH* might play a negative regulatory role in cell motility. Indeed, we found that treatment with small interfering RNA (siRNA) against *MYBPH* (siMYBPH) markedly increased the motility of NCI-H441 cells. Conversely, overexpression of MYBPH reduced Madin-Darby canine kidney (MDCK) cell motility (Figure 3A; Supplementary Figure S3), while that negative effect was cancelled by simultaneous treatment with siMYBPH (Supplementary Figure S4). Similarly, acquisition of the motile phenotype in siMYBPH-treated NCI-H441 cells was clearly demonstrated by results of a scratch assay (Figure 3B) as well as those of a Matrigel invasion assay (Figure 3C), with opposite effects observed in MYBPH-overexpressing MDCK cells. Next, we employed a three-dimensional Matrigel invasion assay and found that MYBPH-overexpressing MDCK cells invaded over a shorter distance and in a more collective manner than the control cells (Figure 3D). Neither siMYBPH treatment of NCI-H441 cells nor forced MYBPH overexpression in MDCK cells had an effect on cell growth (Supplementary Figure S5). We also noted that overexpression of TTF-1 reduced cell motility in HPL1D cells, which was significantly reverted by siMYBPH treatment (Figure 3E), supporting the notion that TTF-1-induced MYBPH negatively affects cell motility.

We also evaluated the effects of MYBPH expression on metastasis using a highly metastatic MYBPH-negative lung cancer cell line, NCI-H460-LNM35 (Kozaki *et al*, 2000). Stable transfectants expressing MYBPH at a level comparable to that in lung adenocarcinoma cell lines (Figure 4A) exhibited significantly reduced lung metastasis (Figure 4B and C), without affecting primary tumour growth (Supplementary Figure S6). Conversely, siMYBPH-treated NCI-H441 cells exhibited increased experimental lung metastasis (Figure 4D and E). In line with the present experimental findings, it was noted that decreased *MYBPH* expression was significantly

 ©2012 European Molecular Biology Organization

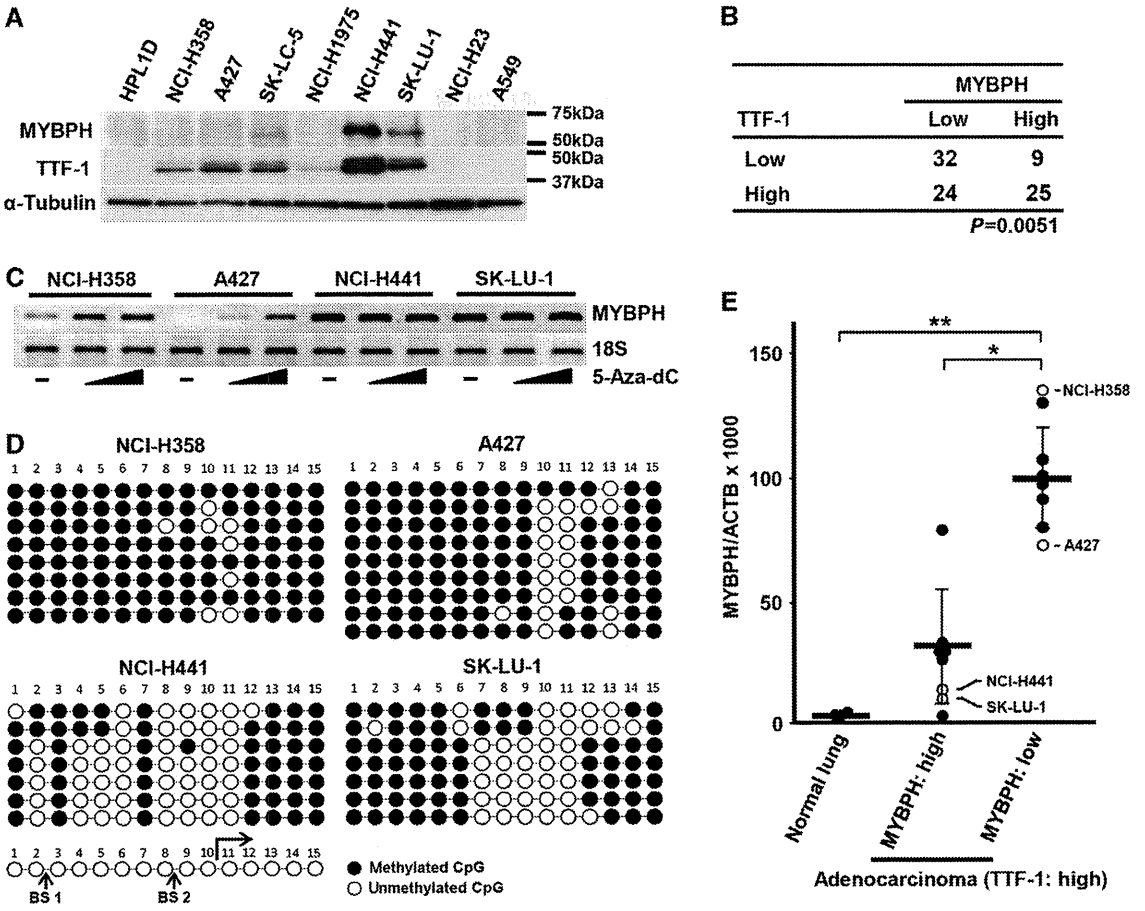

Figure 2 MYBPH expression is inactivated by the promoter CpG methylation. (**A**) Western blot analysis of MYBPH and TTF-1 in lung adenocarcinoma cell lines. (**B**) Correlation between *TTF-1* and *MYBPH* expressions in 90 lung adenocarcinoma specimens. Cases were classified into those above or below the average level of expression. (**C**) Semiquantitative RT–PCR analysis of four cell lines showing *MYBPH* induction in TTF-1-1$^+$/MYBPH$^-$-NCI-H358 and A427 cells after treatment with 5-Aza-dC. 18S served as a loading control. (**D**) Bisulphite sequencing analysis showing dense DNA methylation around BS2 in TTF-1$^+$/MYBPH$^-$-NCI-H358 and A427 cells. (**E**) Methylation-specific PCR analysis of the eighth CpG site in (**D**) using DNA from laser microdissected specimens and representative cell lines, which revealed aberrant DNA methylation in TTF-1$^+$/MYBPH$^-$ lung adenocarcinoma tissues and cell lines. Six cases each of MYBPH-positive and -negative lung adenocarcinomas with abundant TTF-1 expression, along with three normal lung tissues were analysed. Solid circles, clinical samples; open circles, cell lines; bars, mean ± s.d.; $^*P<0.001$; $^{**}P<0.0001$. Figure source data can be found with the Supplementary data.

associated with more apparent invasiveness in surgical specimens obtained from the 90 human lung adenocarcinoma cases (Figure 4F).

MYBPH affects actomyosin organization and cell morphology

We also found that siMYBPH treatment markedly altered the shape of the cells, as they showed a rounded morphology or occasionally bleb-like structures characterized by the appearance of peripheral actomyosin bundles, with clear colocalization of NMHC IIA with the peripheral actin bundles (Figure 5A; Supplementary Figure S7, left). Conversely, overexpression of MYBPH disrupted actomyosin organization as well as the normal morphology in MDCK cells (Figure 5B; Supplementary Figure S7, right). Taken together, these findings strongly support the notion that MYBPH is involved in the regulation of cell shape, motility, invasion, and metastasis.

MYBPH inhibits phosphorylation of RLC through interaction with ROCK1

Our findings strongly suggested that MYBPH is involved in actin organization. We, therefore, analysed changes in the proportion of triton-insoluble F-actin (TIF), a crosslinked meshwork of actin filaments that includes stress fibers (Watts and Howard, 1992), in relation to the level of MYBPH expression. We observed that siMYBPH-treated NCI-H441 cells contained a larger proportion of TIF pools than those treated with the siRNA control. In contrast, *MYBPH*-introduced MDCK cells contained fewer TIF pools than the control cells (Figure 6A).

Phosphorylation of RLC unfolds assembly incompetent NM IIA into assembly competent NM IIA, which is a prerequisite for its assembly and subsequent actomyosin reorganization (Conti and Adelstein, 2008; Vicente-Manzanares *et al*, 2009). In this connection, we found that NCI-H441 knocked down for *MYBPH* exhibited increased RLC phosphorylation, whereas introduction of *MYBPH* reduced the RLC phosphorylation level in MDCK cells (Figure 6B). This finding prompted us to investigate whether MYBPH is involved in the regulation of ROCK-mediated phosphorylation of RLC, since ROCK1 and 2 have been shown to play a central role in the regulation of RLC phosphorylation as downstream effectors of RhoA (Conti and Adelstein, 2008; Vicente-Manzanares *et al*, 2009). *In-vitro* protein–protein binding

©2012 European Molecular Biology Organization

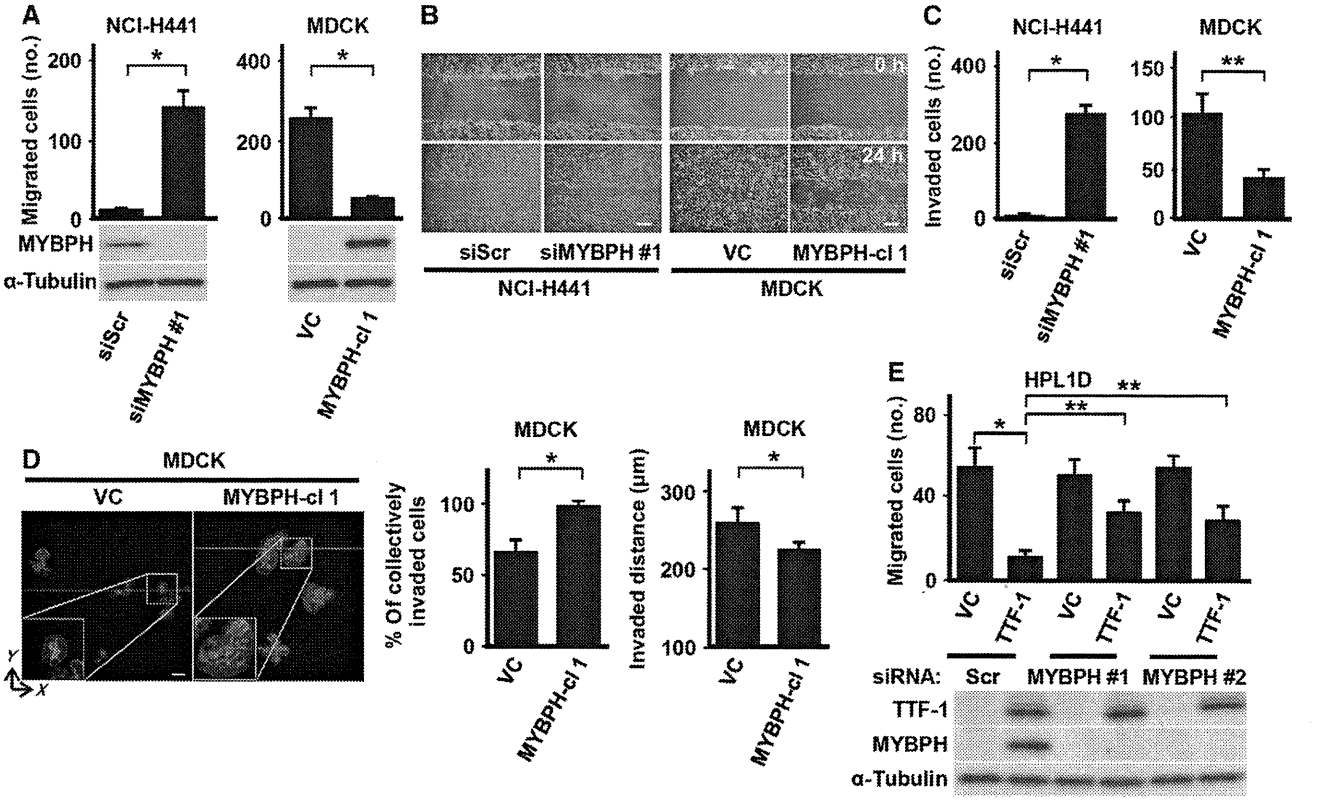

Figure 3 MYBPH reduces cell motility and invasion *in vitro*, and increases collective cell migration. (**A**) Motility assay showing increased *in-vitro* motility by MYBPH knockdown in NCI-H441 cells as well as reduced motility in stable MYBPH transfectant of MDCK cells. Three independent experiments were performed in triplicate. siMYBPH, siRNA against MYBPH; MYBPH-cl 1, MYBPH-transfected clone; bars, mean ± s.d.; $*P<0.01$. Results of corresponding western blot analysis of MYBPH are shown below. (**B**) Scratch assay showing increased *in-vitro* motility by MYBPH knockdown in NCI-H441 cells as well as reduced motility in stable MYBPH transfectant of MDCK cells. Photographs were taken at 24 h after scratch injury. Bars indicate 200 μm. (**C**) Matrigel invasion assay showing increased *in-vitro* invasion by MYBPH knockdown in NCI-H441 cells as well as reduced invasion in stable MYBPH transfectant of MDCK cells. Three independent experiments were performed in triplicate. Bars, mean ± s.d.; $*P<0.001$; $**P<0.01$. (**D**) Three-dimensional Matrigel invasion assay showing collective cell migration and decreased *in-vitro* invasion in stable MYBPH transfectant of MDCK cells. The proportions of cells with collective invasion were evaluated as described in Materials and methods. Data shown represent four independent experiments each counting > 100 cells. White bars indicate 50 μm. Bars, mean ± s.d.; $*P<0.001$. (**E**) Motility assay findings showing reduced *in-vitro* motility in stable TTF-1 transfectants of HPL1D cells, which was cancelled by treatment with siMYBPH. Three independent experiments were performed in triplicate. Bars, mean ± s.d.; $*P<0.01$; $**P<0.05$. The results of corresponding western blot analyses of TTF-1 and MYBPH are shown below. Figure source data can be found with the Supplementary data.

assays were performed to examine whether MYBPH directly interacts with RLC and/or ROCK1 and 2, using a purified His-tagged MYBPH protein with either purified GST-tagged ROCK1, ROCK2, or RLC proteins. Consequently, a direct interaction of MYBPH specifically with ROCK1, but not with RLC, was unexpectedly revealed (Figure 6C). *In-vitro* ROCK kinase assays using purified ROCK1, ROCK2, and RLC proteins in the presence or absence of purified MYBPH protein demonstrated inhibition of ROCK1-mediated RLC phosphorylation by inclusion of MYBPH in the reaction mixture, whereas the presence of MYBPH had no effects on ROCK2-mediated RLC phosphorylation *in vitro*, consistent with the *in-vitro* binding assay results (Figure 6D; Supplementary Figure S8). We also noted that MYBPH was not phosphorylated by either ROCK1 or ROCK2 (Supplementary Figure S8). Immunoprecipitation–western blot (IP–WB) analysis also showed an association of MYBPH with ROCK1 in MYBPH-overexpressing MDCK and NCI-H441 cells, respectively (Figure 6E; Supplementary Figure S9). Overexpression of MYBPH reduced the interaction between ROCK1 and RLC in MDCK, whereas siMYBPH treatment increased their interaction in NCI-H441 cells (Figure 6F). In contrast, the interaction between RhoA and ROCK1 was not affected by MYBPH (Supplementary Figure S10), which appears to be consistent with the interaction of MYBPH with purified GST-tagged ROCK1 protein lacking a RhoA-binding domain near the C-terminus. In addition, IP–WB analysis showed lack of interactions of MYBPH with various RLC kinases (Supplementary Figure S11), including myosin light chain kinase (MLCK), myotonic dystrophy kinase-related CDC42 binding protein kinase alpha and beta (MRCKα and β), citron, and Zipper interacting protein kinase (ZIPK) (Matsumura, 2005).

Further analysis using various deletion mutants of MYBPH showed that the fibronectin type III domain of MYBPH was required for MYBPH binding to ROCK1 (Figure 7A; Supplementary Figure S12). Consistently, a deletion mutant devoid of the fibronectin type III domain did not elicit MYBPH overexpression-induced alterations in cell morphology and actomyosin bundle formation or decreased cell motility in MDCK cells (Figure 7B; Supplementary Figure S13). We also found that MYBPH affects the phosphorylation state of LIMK and cofilin (Figure 7C), which are known to participate in the cascade downstream of ROCK1, thus regulating actin polymerization (Maekawa *et al*, 1999; Yoshioka

©2012 European Molecular Biology Organization

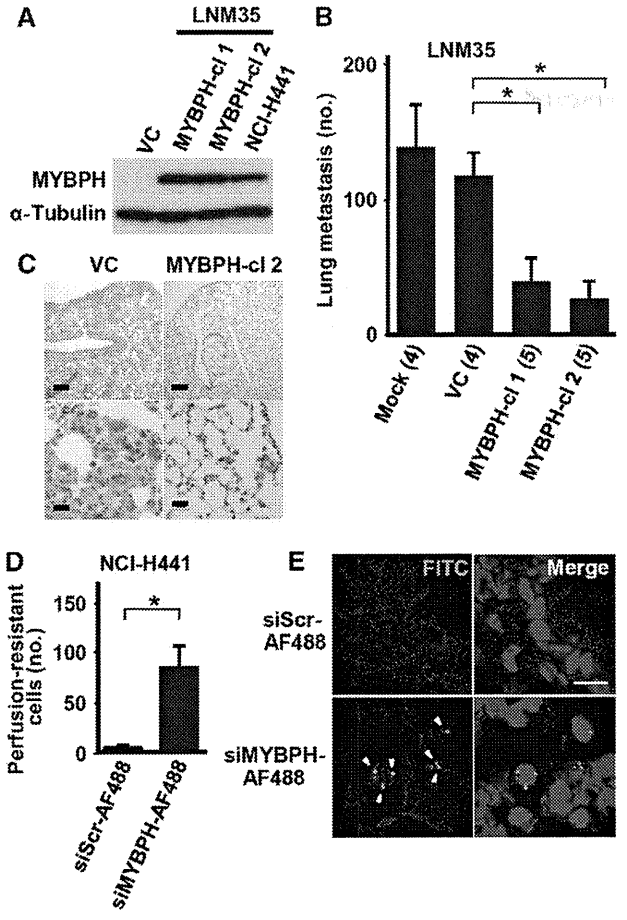

F

Invasion	MYBPH Low	MYBPH High
Definite	46	19
Definite but focal	8	7
Negligible/Negative	2	8

P=0.0065

Figure 4 MYBPH reduces invasion and metastasis *in vivo*. (**A**) Western blot analysis showing expression levels of MYBPH in stable transfectants of NCI-H460-LNM35 (LNM35-MYBPH-cl 1 and -cl 2) expressing MYBPH at a level comparable to that in NCI-H441. (**B**) Decreased lung metastasis in stable MYBPH transfectants of LNM35. Forty days after subcutaneous inoculation, lung metastases were counted. Bars, mean ± s.d.; *$P<0.01$. Numbers in parentheses indicate inoculated mice. (**C**) Representative haematoxylin and eosin-stained images of lung metastases. Bars indicate 200 μm in upper and 20 μm in lower panels. (**D**) Experimental metastasis assay of NCI-H441 cells knocked down for MYBPH with Alexa Fluor 488-conjugated siMYBPH #1 (siMYBPH #1-AF488) (five mice per treatment). Bars, mean ± s.d.; *$P<0.001$. (**E**) Representative fluorescence images of perfusion-resistant cells. Cells were also stained with DAPI (blue). Bars indicate 10 μm. (**F**) Relationships between *MYBPH* expression and invasion status in our previously reported microarray data set of human lung adenocarcinomas. Cases were classified into those above and below the average level of expression. Figure source data can be found with the Supplementary data.

et al, 2003). Consistent with the present findings, increased motility, RLC phosphorylation, and organization of peripheral actomyosin bundles induced by MYBPH knockdown in NCI-H441 cells were significantly, though not completely, counteracted by simultaneous treatment with the ROCK-specific inhibitor Y-27632 (Figure 7D; Supplementary Figure S14). It was also found that increased cell motility and RLC phosphorylation induced by siMYBPH treatment were counteracted by simultaneous treatment with siROCK1, but not with siROCK2 (Figure 7E). Thus, it was demonstrated that MYBPH binds to ROCK1 but not to RLC, leading to inhibition of ROCK1-mediated regulation of actomyosin organization including assembly competence-conferring RLC phosphorylation and activation of the LIMK–cofilin pathway.

MYBPH increases cell–cell contact and collective cell migration

A decrease in ROCK-driven actomyosin contractility enhances cell–cell contact and collective cancer cell invasion (Sahai and Marshall, 2002; Hidalgo-Carcedo *et al*, 2011). Along this line, NCI-H441 cells knocked down for MYBPH migrated mostly as single cells in a three-dimensional invasion assay, which was reverted by simultaneous treatment with Y-27632 (Figure 8A). This siMYBPH-mediated increase in single cell migration was markedly counteracted by simultaneous treatment with siROCK1 (Figure 8B). While one of the hallmarks characterizing collective cell migration is preservation of the integrity of cell–cell contact during movement (Friedl and Gilmour, 2009), MYBPH knockdown markedly decreased cell–cell contact in NCI-H441 cells, as shown in our aggregation assay. This effect was clearly counteracted by a simultaneous treatment with Y-27632 (Figure 8C). Conversely, overexpression of MYBPH reduced MDCK cell aggregation (Figure 8D). Formation of adherence junctions positively regulate cell–cell contacts in epithelial cells (Friedl and Wolf, 2010). Our aggregation assay findings showed that siMYBPH-treated NCI-H441 cells exhibited a readily detectable decrease in E-cadherin staining intensity on the cell surface, which was considerably counteracted by simultaneous treatment with Y-27632 (Figure 8E). Conversely, overexpression of MYBPH increased E-cadherin intensity in MDCK cells similarly examined by an aggregation assay (Supplementary Figure S15). Interestingly, western blot analysis demonstrated similar levels of E-cadherin expression irrespective of MYBPH state. Taken together, the present findings indicate that TTF-1-inducible MYBPH inhibits ROCK1 through direct interaction, which in turn negatively regulates actomyosin organization, leading to decreased cell motility, invasion, and metastasis (Figure 9).

Discussion

The present findings indicate that *MYBPH*, which we identified here as a direct transcriptional target of *TTF-1*, plays multiple roles in negative regulation of actomyosin organization. Among the various myosin binding proteins, a cardiac isoform of *MYBPC* (*cMYBPC*) has been the focus of intense research activities, because of its direct involvement in cardiovascular diseases such as familial hypertrophic cardiomyopathy (Bonne *et al*, 1995; Watkins *et al*, 1995; Richard *et al*, 2003). While *MYBPH* and *cMYBPC* possess significant homology at their carboxyl termini, *MYBPH* lacks a region homologous to the amino terminal half of *cMYBPC*, which is required for inhibition of myosin functions. To date, very little is known about the functions of *MYBPH*, even in regard to its interaction with muscle myosin (Yamamoto, 1988; Welikson and Fischman, 2002), with virtually nothing reported regarding its roles in non-muscle cells.

©2012 European Molecular Biology Organization

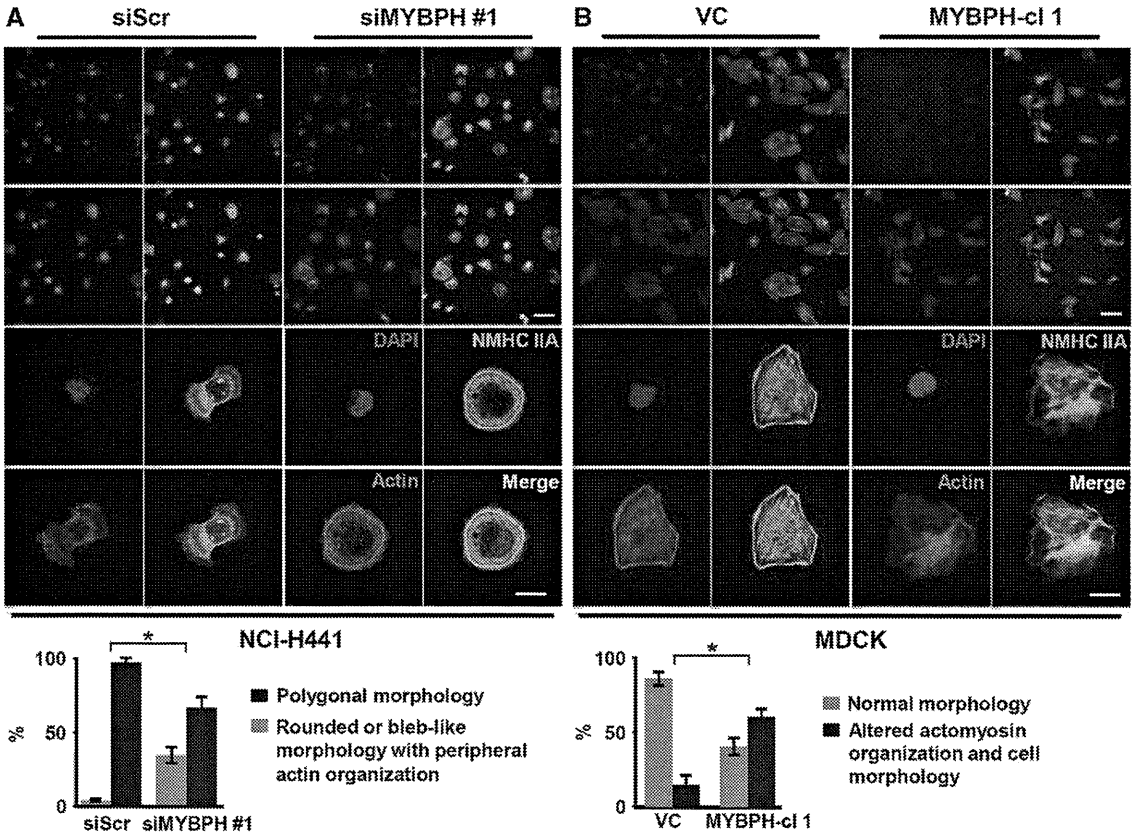

Figure 5 MYBPH affects actomyosin organization and cell morphology. (**A**) Top panels: immunofluorescence staining for DAPI (blue), actin (red), and NMHC IIA (green) in NCI-H441 cells treated with siScr or siMYBPH. Bars indicate 100 μm in top and 10 μm in bottom panels. Bottom panel: proportions of cells according to morphology. Data shown represent three independent experiments each counting >100 cells. Bars, mean ± s.d.; $^*P<0.001$. Results with an additional siMYBPH are also shown in the left panels of Supplementary Figure S7. (**B**) Top panels: immunofluorescence staining for DAPI (blue), actin (red), and NMHC IIA (green) in MDCK cells stably transfected with empty or MYBPH-expressing vectors. Bars indicate 100 μm in top and 10 μm in bottom panels. Bottom panel: proportions of cells according to morphology, which were determined as shown in (**A**). Bars, mean ± s.d.; $^*P<0.001$. Results obtained with an additional independent clone are shown in the right panels of Supplementary Figure S7.

In this study, we found that MYBPH inhibits assembly competence-conferring RLC phosphorylation as well as activating phosphorylation of LIMK. MYBPH unexpectedly executes such inhibitory activities by direct physical interaction with ROCK1 rather than with RLC, which results in inhibition of ROCK1 kinase activity. ROCK1 is a downstream effector of RhoA that is crucially involved in cell morphogenesis and motility, as well as in cancer progression (Itoh *et al*, 1999; Sahai and Marshall, 2003; Wilkinson *et al*, 2005; Wong *et al*, 2008). To date, however, very few examples have been reported as negative regulators of ROCK1. While RhoE has been shown to inhibit ROCK1 by competing with RhoA for ROCK1 (Riento *et al*, 2003), MYBPH directly binds to and interferes with ROCK1, which in turn inhibits RLC phosphorylation. Our findings thus add MYBPH to the small list of negative ROCK1 regulators, suggesting a complex nature of the negative regulatory mechanisms of ROCK1.

It is interesting that marked distinctions were observed in terms of specificities of the binding and inhibitory capabilities of MYBPH towards ROCK1 and ROCK2. Along line, it is important to note that RhoE binds to ROCK1 but not to ROCK2 and inhibits its function, resulting in loss of stress fiber formation (Riento *et al*, 2003). It was also reported that siRNA-mediated ROCK1 knockdown results in loss of stress fibers, in contrast to lack of such effects in cells knocked down for ROCK2 (Yoneda *et al*, 2005). Together, these findings indicate that ROCK1 plays a major role in stress fiber formation and are in line with the present findings of actomyosin regulation by MYBPH through ROCK1 inhibition.

Considering that ROCK1 also mediates regulatory phosphorylation of various other molecules, such as endothelial nitric oxide synthase (eNOS) and collapsin response mediator protein 2 (CRMP2), and is involved in a wide range of disease states including vasospasms, pulmonary hypertension, and nerve injury (Etienne-Manneville and Hall, 2002; Riento and Ridley, 2003), it would be interesting to investigate whether MYBPH might be involved in such disease states as a regulator of ROCK1. In addition, given that collective cell migration plays an important role in various physiological settings including morphogenesis, tissue regeneration, and repair of wounded epithelial tissues (Kimura *et al*, 1996; White *et al*, 2001; Pogach *et al*, 2007), it is of note that changes in MYBPH expression alter actomyosin organization, and consequently affect collective cell migration, especially when considering that TTF-1 is a master regulatory transcription factor involved in peripheral lung development (Kimura *et al*, 1996; Yatabe *et al*, 2002) and that type II pneumocyte hyperplasia, a reconstitution process of the alveolar lining, is associated with increased TTF-1expression (White *et al*, 2001; Pogach *et al*, 2007).

©2012 European Molecular Biology Organization

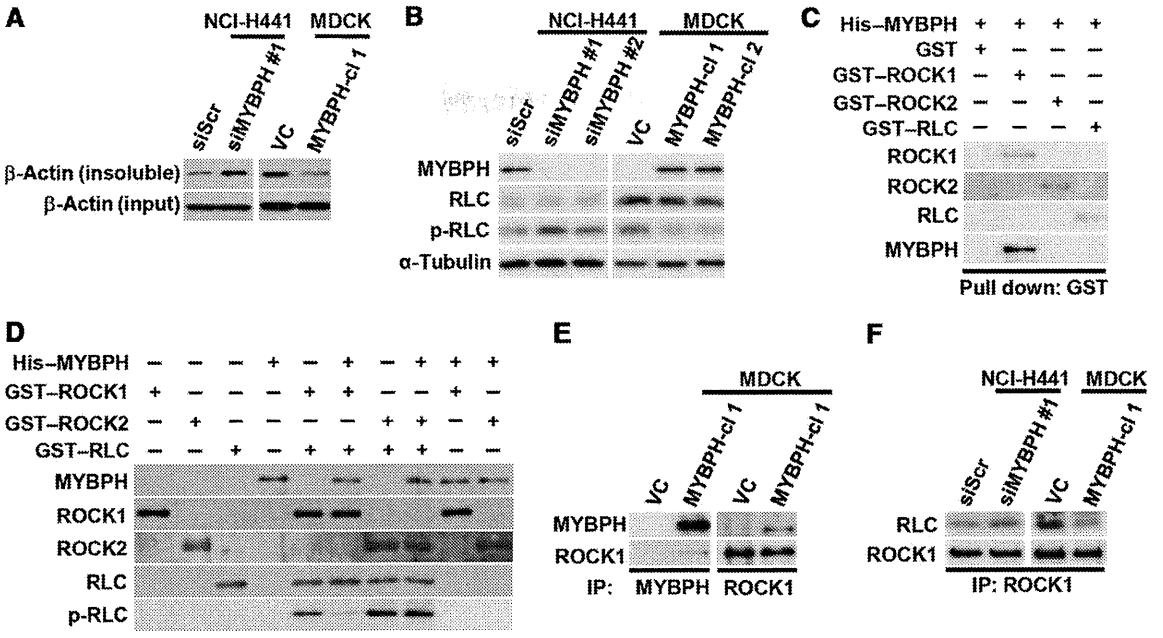

Figure 6 MYBPH inhibits phosphorylation of RLC through interaction with ROCK 1. (**A**) Actin assembly assay showing an increase in triton-insoluble unassembled F-actin (TIF) in siMYBPH-treated NCI-H441 cells as well as opposite effects by MYBPH introduction in MDCK cells. (**B**) Western blot analysis showing induction of RLC phosphorylation by MYBPH knockdown in NCI-H441 cells as well as reduction in MYBPH transfectants of MDCK cells. p-RLC, phospho-RLC (T18/S19). (**C**) *In-vitro* protein–protein binding assay results showing interaction of purified MYBPH with ROCK1, but not with ROCK2 or RLC. (**D**) *In-vitro* ROCK kinase assay using purified RLC protein as a substrate, showing inhibition of ROCK1-mediated RLC phosphorylation by MYBPH. (**E**) Immunoprecipitation–western blot (IP–WB) analysis showing co-immunoprecipitation of MYBPH with ROCK1 in MDCK cells expressing exogenous MYBPH. (**F**) IP–WB analysis showing increased interaction between ROCK1 and RLC by siMYBPH treatment in NCI-H441 cells. Conversely, their reduced interaction was seen in MDCK cells stably transfected with MYBPH. Figure source data can be found with the Supplementary data.

Our results clearly demonstrate that MYBPH negatively regulates cell motility, invasion, and metastasis. Thus, it is quite conceivable that *MYBPH* induction by *TTF-1* is deleterious for lung adenocarcinoma progression, which is thereby inactivated by promoter DNA methylation in a fraction of *TTF-1*-positive lung adenocarcinomas. This finding in turn resolves a question arising from previous observations that a high level of *TTF-1* expression, which we and others have identified as a lineage-survival oncogene in lung adenocarcinoma (Kendall *et al*, 2007; Tanaka *et al*, 2007; Weir *et al*, 2007; Kwei *et al*, 2008), is paradoxically associated with favourable prognosis (Anagnostou *et al*, 2009). We note that during the preparation of this manuscript, Jacks and colleagues reported that TTF-1 downregulation was associated with tumour progression and acquisition of metastatic ability, in association with derepression of HMGA2 in a lung adenocarcinoma model of mutant K-ras/p53 conditional knockout (Winslow *et al*, 2011). Our findings further indicate that MYBPH plays a crucial role as a positively regulated downstream effector of TTF-1, with capabilities for inhibiting cancer cell motility, invasion, and metastasis. Thus, both transcriptional activation and repression by TTF-1 appear to be engaged in conferring a less aggressive phenotype, despite its opposing role as a lineage-survival oncogene in TTF-1-positive lung adenocarcinomas (Kendall *et al*, 2007; Tanaka *et al*, 2007; Weir *et al*, 2007; Kwei *et al*, 2008).

Materials and methods

Cell lines

The derivation, characteristics, and culture conditions of the human lung adenocarcinoma cell lines utilized, and the immortalized human lung epithelial cell line HPL1D as well as the highly metastatic NCI-H460-LNM35 (LNM35) lung cancer cell line were previously reported (Masuda *et al*, 1997; Kozaki *et al*, 2000; Tanaka *et al*, 2007). An MDCK cell line was purchased from RIKEN Cell Bank and maintained in Dulbecco's Modified Eagle's Medium containing 10% fetal bovine serum.

Antibodies, reagents, and oligonucleotide primers

The anti-TTF-1 antibody for western blot analysis was purchased from DAKO; anti-TTF-1 for the ChIP assay from Thermo; anti-MYBPH from Abnova; anti-E-cadherin from BD Transduction Laboratories; anti-GST and anti-His from MBL; anti-NMHC IIA, anti-MLCK, anti-β-actin, and anti-α-tubulin from Sigma-Aldrich; anti-ROCK1, anti-ROCK2, anti-RLC, anti-phospho-RLC (T18/S19), anti-cofilin, anti-phospho-cofilin (S3), anti-phospho-LIMK1 (T508)/LIMK2 (T505), anti-mouse IgG, and anti-rabbit IgG from Cell Signalling Technology; anti-Citron from Novus; anti-RhoA, anti-MRCK-α, and anti-MRCK-β from Santa Cruz; and anti-ZIPK from Calbiochem. ROCK-specific inhibitor Y-27632 was also purchased from Calbiochem. The sequences of the oligonucleotide primers used for PCR and sequencing are provided in Supplementary Table S1.

DNA constructs

The expression construct of full-length human *TTF-1* (pCMV puro-TTF-1) was previously described (Tanaka *et al*, 2007). Full-length human *MYBPH* cDNA (OpenBio) was inserted into a pCMV-puro vector and the entire open reading frame of the resultant construct (pCMVpuro-MYBPH) was thoroughly sequenced. Transfection was performed using FuGENE6 (Roche), followed by puromycin selection.

Microarray data

RNA was extracted from HPL1D cells transiently transfected with TTF-1 or an empty vector followed by puromycin selection for 3 days, and analysed in duplicate (GSE26721), using a low RNA fluorescent linear amplification kit and 44K whole human genome microarrays (Agilent Technologies), essentially as described previously (Tomida *et al*, 2009). Our previously obtained micro-

©2012 European Molecular Biology Organization

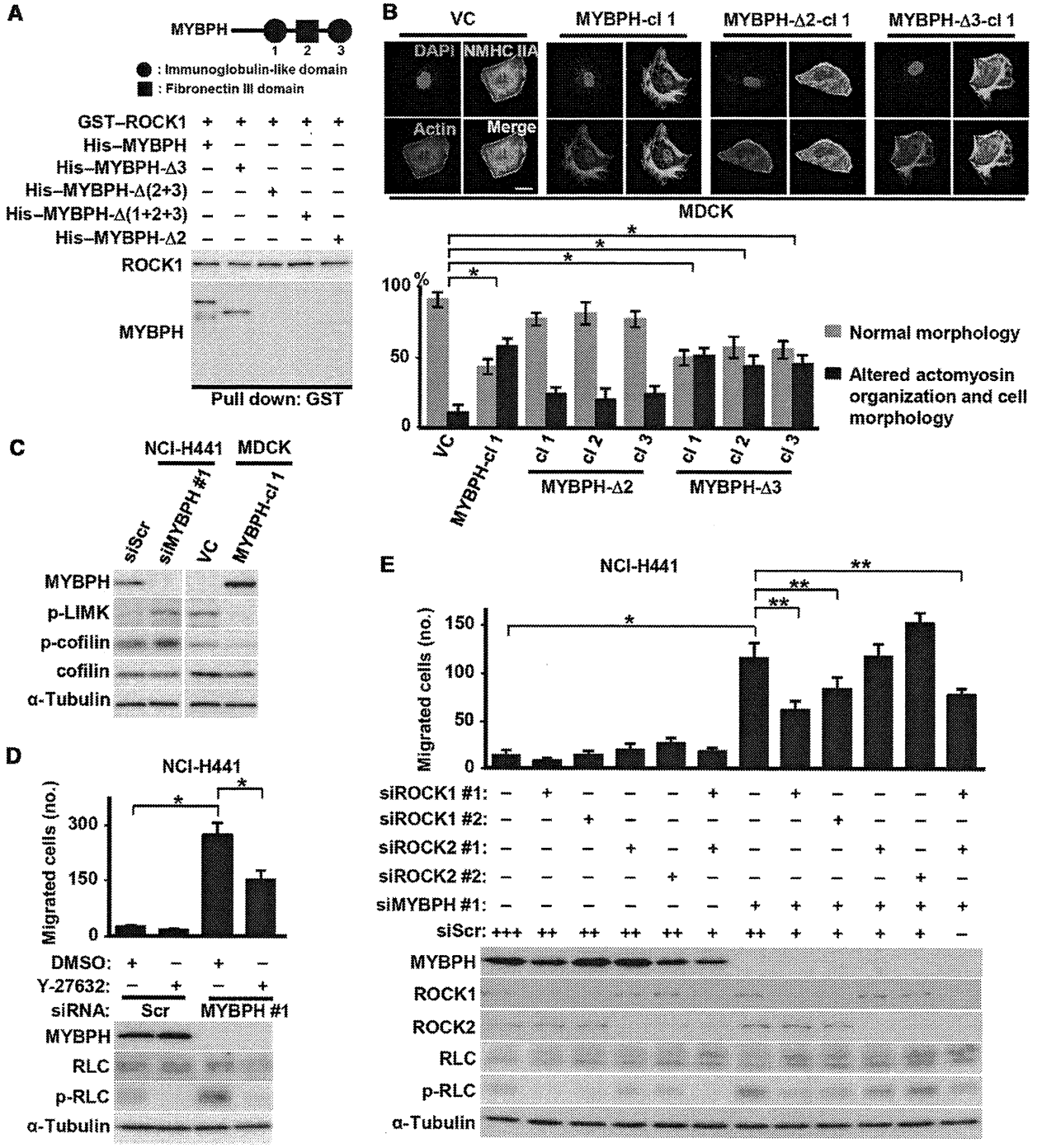

Figure 7 MYBPH knockdown-induced effects on actin bundle formation, cell motility and RLC phosphorylation are alleviated through ROCK1 binding and inhibition. (**A**) Top panel: schematic representation of domain organization of MYBPH. Bottom panel: *in-vitro* protein–protein binding assay showing requirement of a fibronectin type III domain of MYBPH for its binding with ROCK1. Western blot analysis of His-tagged MYBPH-wt, -Δ3, -Δ(2 + 3), -Δ(1 + 2 + 3), and -Δ2 proteins are shown in Supplementary Figure S12. (**B**) Top panels: immunofluorescence staining for DAPI (blue), actin (red), and NMHC IIA (green) in MDCK cells stably introduced with an empty vector (VC), or MYBPH expression constructs of wild-type or deletion mutants lacking either fibronectin type III (MYBPH-Δ2) or immunoglobulin-like domains. Bars indicate 10 μm. Bottom panel: proportions of cells according to morphology, which were determined as shown in Figure 5A. Bars, mean ± s.d.; $^*P<0.001$. (**C**) Western blot analysis showing induction of LIMK and cofilin phosphorylation by MYBPH knockdown in NCI-H441 cells as well as reduction in MYBPH transfectant of MDCK cells. p-LIMK, phospho-LIMK1 (T508)/LIMK2 (T505); p-cofilin, phospho-cofilin (S3). (**D**) Top panel: partial cancellation of the MYBPH knockdown-induced motility by a simultaneous treatment with a ROCK-specific inhibitor Y-27632 in NCI-H441 cells. Bars, mean ± s.d.; $^*P<0.01$. Bottom panel: representative western blot images for RLC phosphorylation. (**E**) Top panel: partial cancellation of MYBPH knockdown-induced motility by simultaneous treatment with siRNAs against ROCK1 in NCI-H441 cells. Bars, mean ± s.d.; $^*P<0.01$; $^{**}P<0.05$. Bottom panel: representative western blot images for RLC phosphorylation. siRNA concentrations: +, 40 nM; + +, 80 nM; + + +, 120 nM. Figure source data can be found with the Supplementary data.

array data of 90 lung adenocarcinoma cases (Takeuchi *et al*, 2006; GSE11969) were used to analyse the association of *MYBPH* expression with *TTF-1* expression as well as with various clinical parameters.

siRNA treatment

siRNA duplexes targeting TTF-1 (siTTF-1) and MYBPH (siMYBPH #1 and #2 as well as siMYBPH-AF488, Alexa Fluor 488-conjugated siMYBPH #1) and a negative control (siScr) were obtained from

©2012 European Molecular Biology Organization

Sigma Genosys, while siRNA duplexes targeting ROCK1 (siROCK1 #1 and #2) and ROCK2 (#1 and #2) from Invitrogen. Transfection of each siRNA at 40 nM was performed using Lipofectamine RNAiMAX (Invitrogen). Cells were harvested at 48 h after transfection for each assay. The sequences of the siRNAs are provided in Supplementary Table S1.

Western blot analysis

Western blot analysis was performed according to standard procedures using Immobilon-P filters (Millipore) and an Enhanced Chemiluminescence system (GE Healthcare). NCI-H441 cells were treated with Y-27632 (5 μM) for 15 min before.

IP–WB analysis

Cells (2×10^7) were lysed with modified RIPA buffer containing protease inhibitor cocktail Tablets (Roche) and incubated with each antibody overnight at 4°C, followed by addition of protein G Sepharose (GE Healthcare) and subsequent incubation for an additional 1 h. The immunoprecipitates were analysed by western blot analysis.

Dual-luciferase reporter assay

An MYBPH *luciferase* reporter construct was generated using a pGL4 basic reporter vector (Promega) and a PCR-amplified 1.0-kb genomic fragment from the MYBPH promoter region. Mutant vectors carrying deletions at the predicted binding sites for *TTF-1* and *NKX2-5* were constructed using a QuikChange site-directed mutagenesis kit (Stratagene). HPL1D cells (3.0×10^5) transiently expressing *TTF-1* were transfected with each pGL4 vector (1.8 μg) together with a pRLTK vector (0.2 μg), then the cell lysates were collected after 48 h. Luciferase reporter activities were determined using a Dual-Luciferase Reporter Assay System (Promega). Firefly luciferase activity was normalized with that of Renilla luciferase.

ChIP assay

NCI-H441 cells (1.0×10^8) were harvested after crosslinking with 1% formaldehyde. Chromatin was sheared by sonication to an average length of 500–600 bp, followed by immunoprecipitation with a TTF-1-specific antibody. After reversal of crosslinking, immunoprecipitated chromatin was subjected to PCR using primers for the predicted binding sites of *TTF-1* and *NKX2-5* as well as those for an unrelated genomic region as a negative control.

Treatment with 5-aza-2′-deoxycytidine

Cells ($1.0–1.5 \times 10^5$) were incubated with 1 or 2 μM of 5-aza-2′-deoxycytidine (5-Aza-dC; Sigma) for 5 days. Media were changed every 24 h. Semiquantitative PCR was performed using primers for amplification of the coding region of MYBPH.

Bisulphite sequencing analysis

Bisulphite conversion of genomic DNA was performed using MethylEasy Xceed™ (Human Genetic Signatures), according to the manufacturer's instructions. The MYBPH promoter region was amplified using nested primers and the resultant PCR products were cloned into pGEM-T easy vectors (Promega), followed by sequencing of randomly selected clones.

Laser microdissection and MSP

Cancer cells were microdissected from 20 μm thick frozen sections using a Leica LMD 7000 Laser Micro-dissection system (Leica Microsystems). Bisulphite-modified DNA was used as a template for SYBR Green (Applied Biosystems)-based real-time PCR, with primers designed for specific detection of methylated DNA at a CpG (#8) close to the TTF-1-binding consensus sequence of the *MYBPH* promoter and a promoter region without CpG sites of the reference gene, *ACTB*. The methylation level in the *MYBPH* promoter was determined as the ratio of methylation-specific PCR-amplified *MYBPH* gene to *ACTB* reference gene, and then multiplied by 1000 for easier tabulation.

In-vitro motility, invasion, scratch, and MTT assays

In-vitro motility and invasion assays were essentially performed as previously described (Kozaki *et al*, 2000). For each assay, 1×10^5 MDCK cells, 1.5×10^5 NCI-H441, and HPL1D cells were added to the upper chambers, then incubated for 24, 36 and 36 h, respectively. NCI-H441 cells were treated with Y-27632 (5 μM) for 15 min before incubation. For a scratch assay, 1.5×10^6 cells were plated in 6-well plates. After 24 h of incubation, a single linear wound was created with a 200-μl pipette tip. An MTT assay was performed with TetraColor One (Seikagaku) according to the manufacturer's instructions.

Three-dimensional Matrigel invasion assay and immunostaining

One hundred microlitres of Matrigel (BD Biosciences) was prepared on 18 × 18 mm coverslips in 6-well plates, on which 2×10^5 cells were plated and cultured for 48 h, followed by fixation with 3.7% formaldehyde for 30 min and post-fixing with 0.1% Triton X-100 for 30 min at room temperature (RT). Cells were incubated with blocking buffer (1% BSA in PBS) overnight at 4°C and were visualized by staining with Alexa-conjugated phalloidin (Molecular Probes). The coverslips were mounted onto slides using Fluoromount (Diagnostic BioSystems) and analysed using an A1 Rsi confocal microscope (Nikon). The invasion distance was defined as that between the slide glass (top of the Matrigel) and the centre of fluorescence intensity, and measured using MetaMorph (Molecular Devices) software. The extent of collective cell migration was defined as the ratio of collective cells (⩾5 cells) to total cell number. Data shown represent three independent experiments, with >100 cells counted in each.

In-vivo metastasis assay

LNM35 cells (1.0×10^7) in 0.1 ml of serum-free RPMI-1640 medium were injected into subcutaneous tissues of the right groin of 6-week-old female SCID mice. Forty days after inoculation, the mice were euthanized, and their lungs and subcutaneous tumours resected, weighed, and fixed with 10% formaldehyde. Lung-metastatic nodules were examined under a dissecting microscope. An experimental metastasis assay following tail vein injection of tumour cells was performed, essentially as described by Shibue and Weinberg (2009). NCI-H441 cells were transfected with either Alexa Fluor 488-conjugated siScr (siScr-AF488) or -siMYBPH #1 (siMYBPH-AF488) as described above, then the transfectants were harvested 48 h later. Cells at 1.0×10^6 in 0.1 ml of PBS were injected into tail veins of 6-week-old female SCID mice. Five days after injection, the mice were euthanized, then 6 ml of PBS was injected into the right ventricle for perfusion of the lung microvasculature. The perfused lungs were embedded in OCT (Sakura), sectioned (thickness 10 μm) with a Leica CM3050 (Leica Microsystems), and fixed using Fluoromount. Perfusion-resistant cells were determined by direct counting in the sections using an A1 Rsi confocal microscope.

Immunostaining

Cells (0.5×10^5) were plated on 18 × 18 mm coverslips in 6-well plates and cultured for 12 h. NCI-H441 cells were treated with Y-27632 (5 μM) for 15 min before plated. The cells were fixed by incubating with 3.7% formaldehyde for 10 min at RT, followed by post-fixing with 0.1% Triton X-100 for 10 min at RT. Cells were incubated with blocking buffer overnight at 4°C, followed by another incubation with antibodies (diluted in blocking buffer) for 60 min at RT. After treatment with Alexa-conjugated secondary antibodies (Molecular Probes) for 60 min at RT, the coverslips were mounted onto slides using Fluoromount, and analysed using an A1 Rsi confocal microscope.

Actin assembly assay

Cells were lysed with buffer containing 1% Triton X-100, 10 mM EGTA, 40 mM NaCl, 10 mM imidazole, and a protease inhibitor cocktail (Roche) at 4°C. The lysates were centrifuged at 15 000 × *g* for 5 min at 4°C, then the pellets were washed, dissolved in 1 × SDS sample buffer, and subjected to western blot analysis with an anti-actin antibody. Three independent experiments were performed in triplicate, with similar results obtained.

Preparation of recombinant proteins

His-tagged MYBPH-wt, -Δ3, -Δ(2 + 3), -Δ(1 + 2 + 3), and -Δ2 proteins were expressed in Sf9 insect cells using a Gateway system (Invitrogen), according to the manufacturer's instructions. Recombinant His-tagged MYBPH-wt, -Δ3, -Δ(2 + 3), -Δ(1 + 2 + 3), and -Δ2 proteins were purified using imidazole-affinity chromatography. Recombinant GST-tagged ROCK1 (amino acids 17–535) and GST-tagged ROCK2 (amino acids 5–554) were purchased from Sigma. GST-tagged RLC and GST were from Abnova.

©2012 European Molecular Biology Organization